Numerical prediction of dropwise condensation performances on hybrid hydrophobic-hydrophilic surfaces

Numerical prediction of dropwise condensation performances on hybrid hydrophobic-hydrophilic surfaces

Giulio Croce[1] **and Nicola Suzzi**[1] **and Paola D'Agaro**[1]

[1]DPIA - Dipartimento Politecnico di Ingegneria e Architettura - Universitá di Udine - Via delle Scienze - 33100 - Udine (UD) - Italy

E-mail: giulio.croce@uniud.it, suzzi.nicola@spes.uniud.it, paola.dagaro@uniud.it

Abstract. The use of hybrid surfaces, alternating hydrophobic and hydrophilic (or less-hydrophobic) areas, has been recently proposed as a valuable tool for dropwise condensation performances enhancement. The hydrophilic region, in particular, is designed in order to promote the removal of the droplet from the hydrophobic region, reducing their average size and thus increasing the heat transfer performance. Here, dropwise condensation on heterogeneous surfaces composed by a texture of alternating hydrophobic and hydrophilic (or less-hydrophobic) vertical strips is numerically investigated through a Lagrangian-based phenomenological model, originally developed to study droplet evolution in the framework of in-flight icing phenomenon. The effects of droplet nucleation, growth, coalescence and motion are implemented. The model is extended to the case of curved surface. In order to properly assess the hybrid surface, however, a better knowledge of the interaction between the droplet and the film is required. Thus, additional numerical simulations are carried out using an in-house Eulerian full solver of the liquid film layer, in order to understand the migration mechanism of a drop between two different wettability regions. This will give useful information for a proper implementation of the effect of hydrophilic strips in the phenomenological Lagrangian model. A parametric analysis allows to find the optimal geometric configuration of the hybrid pattern, leading to maximum heat transfer performance, for a given set of wettability properties, nucleation density and condensation rate per unit area. Comparison with experimental data from the available literature ensures the capability of the current Lagrangian model to properly catch the physics behind dropwise condensation process on both planar and curved hybrid surfaces. The uncertainty of the estimate of some model input parameter and their influence on the computed solution are be also discussed.

1. Introduction

The evolution of a droplet pattern over a solid substrate is involved in a number of engineering applications. In particular, the droplet size and distribution have a great impact on: heat transfer performances of HVAC finned dehumidification devices [1]; safety issues related to both the airplane inflight icing [2] and the visibility through fogged automotive windshield [3–5]; defogging process of refrigerated cabinets door [6]. When condensation is involved, as it happens in most of HVAC applications, dropwise mode is much more efficient than filmwise one, allowing for heat transfer enhancement. Thus, various methods have been implemented in order to promote dropwise condensation (DWC). In fact, effective DWC can be achieved through micro and nano-structured hydrophobic and superhydrophobic surfaces [7]. The heat transfer surface may be entirely nonwettable or an hybrid one, characterized by a pattern of hydrophobic and hydrophilic (or less hydrophobic) regions. The hybrid surfaces design has been introduced in order to ensure higher replenishment frequency at smaller drop diameter. The existence of optimal geometrical configurations is demonstrated by literature experimental results [8, 9]. Most of the above mentioned applications are inherently multiscale problems: the smaller

scales range from the mesoscale related to the droplet size down to the molecular scale characterizing the interaction between liquid and solid substrate; on the other side, the larger macroscales include the fully 3D thermofluidodynamic problem, driving the shear stress over the airplane wings in case of inflight-icing phenomena or the condensation heat transfer rate over the whole surface of a finned dehumidifier. Thus, decoupling droplet dynamics from the fully 3D problem is required in order to reduce computational cost when the numerical approach is adopted.
The droplet pattern evolution is here predicted via an efficient phenomenological model, based on a simplified modeling of the smaller scale (via imposition of contact angle and nucleation density); adopting a Lagrangian approach, the history of each droplet is followed in order to provide, via postprocessing of the droplets population, statistically relevant information to the macroscale problem. The mathematical procedure, developed and validated for the prediction of droplet pattern in inflight-icing problems [2] and moisture condensation in finned dehumidifier [1], was extended to pure steam condensation over plane or cylindrical surfaces by the authors in [10]. However, it was not possible to replicate the details of the interaction between the discrete droplets and the hydrophilic strip, experimentally proved in [8, 9]. To do so, a numerical investigation is conducted using a fully Eulerian solver of the governing lubrication equation, looking for the hydrodynamics driving the drop absorption process. The effect of hydrophilic strip is implemented in the phenomenological model, using the information provided by the fluid dynamics simulations. Also, new mechanisms, such as the dependence of the contact angle hysteresis on the external forces, are added. Test cases experimentally investigated in the available literature are replicated, in order to assess the accuracy and the uncertainty of the proposed model. The effect of the geometrical configuration of the hybrid surface is investigated.

2. Mathematical model

The prediction of the thermal performances of hybrid surfaces requires a simulation of the evolution of the droplet population, taking into account the wetting properties of the surface. Since a multiphase numerical computation quickly becomes unpractical due to the required mesh refinement, a possible choice is to follow each individual droplet evolution from nucleation to shedding adopting a Lagrangian approach. The process is simplified with a phenomenological model that describes the main steps of the evolution, namely nucleation, growth, coalescence and shedding. The droplet shape is approximated with a spherical cap, defined by a constant contact angle along its contour.
The modeling process, implemented in a in-house `FORTRAN` code, can be summarized in the following steps: generation of nuclei at random locations (only dry spots are active); growth of the whole droplets population due to condensation; coalescence check and hydrophilic strip absorption; droplet movement check, including coalescence along moving path; next time step.
Nucleation step requires the knowledge of the actual number of nucleation sites, which is not easy to determine in most of the practical applications. Rose correlation [11],

$$N = 0.037\, {r_n}^{-2} \tag{1}$$

estimates the nucleation density $N\,(\mathrm{m}^{-2})$ as a function of the nucleation radius r_n. However, Eq. (1) is known to overestimate the real value of N, which ranges between 10^9 to 10^{11} in practical applications [12]. Since coalescence is significant when droplet radius approaches a critical value [11],

$$r_{cr} \sim (4N)^{-1/2} \tag{2}$$

it can be assumed that newly nucleated drops grow independently one from each other until $r = r_{cr}$. Thus, the very first stage of droplet growth is neglected and the initial radius of the new drops is set in all the computations to a safe value of $r_0 = r_{cr}/4$ without losing accuracy. To ensure consistency with the physical process, the integration time step corresponds to the time required by the newly nucleated drop to grow from the nucleating radius to the imposed initial radius [10],

$$\Delta t = \frac{r_0 - r_n}{u_r},\; u_r = \frac{dr}{dt} = \frac{q''_c}{\rho\,\lambda}\,\frac{3}{\left(2+\cos\bar{\theta}\right)\left(1-\cos\bar{\theta}\right)} \tag{3}$$

q_c'' being the condensation heat flux per unit area, λ the condensation latent heat, ρ the liquid density and $\bar{\theta}$ the averaged contact angle along drop perimeter. The drop growth velocity due to condensation u_r depends on the imposed q_c'', which in turns is evaluated as a function of the substrate subcooling ΔT_{sc}. Droplets also grow because of coalescence. Coalescence occurs when overlapping between adjacent droplets is detected. The volume of the resulting drop will be the sum of the volumes of the pre-merged drops and will be located at the center of mass of the two pre-merged drops.
Drops are subjected to external forces, given by gravity and aerodynamic drag, the last contribution arising when the wetting surface is exposed to a gas flow. Thus, the drop becomes non-spherical and is characterized by an hysteresis. The actual contact angle, which ranges between θ_{min} and θ_{max}, is a function of the azimuthal angle ψ, according to [13, 14]. Since the condensing droplet is growing, it is reasonable to assume that the maximum value of the contact angle is equal to the advancing contact angle, $\theta_{max} = \theta_a$, while the actual value of θ_{min} depends on the drop deformation, i.e. on the magnitude of the external forces. The balance between drag, gravitational force (projected along solid surface) and rigidity force (i.e. the surface tension force acting along moving axis due to contact angle hysteresis) allows to determine the actual θ_{min}. Since the drag force is not considered in the current study, the following expression, taking into account of gravity and surface tension, is implemented,

$$\cos\theta_{min} = \cos\theta_a + \frac{F_g}{F_\sigma} \tag{4}$$

$$F_\sigma = \frac{24}{\pi^3}\,\sigma\, d_b \;;\; F_g = \rho\, g\, V_{drp}\,\sin\alpha \tag{5}$$

α being the angle between the substrate outward normal and the gravity vector. The fully derivation of both the gravitational force F_g and the surface tension force F_σ used in Eq. (4) can be found in [15, 16]. The averaged drop contact angle,

$$\bar{\theta} = \frac{1}{\pi}\int_0^\pi \theta\, d\psi \simeq \frac{\theta_a + \theta_{min}}{2} \tag{6}$$

is updated at each time step for each drop and used to evaluate coalescence condition, drop radius, drop free surface and rigidity force. The motion of the drop is triggered when the computed θ_{min} is lower than the receding contact angle θ_r. In such a case, θ_r is chosen as the minimum contact angle and a power balance between gravity force work Φ_g, surface tension work Φ_σ and viscous dissipation Φ_v, given by the sum of laminar viscous dissipation at the core flow and wedge dissipation, is imposed in order to compute drop velocity, as explained in [1, 17].
The implemented procedure is suitable for both plane and tube surfaces. In the latter case, α depends on the position along the tube circumferential coordinate. The computational domain, which is periodic, is given by the unwrapped surface of a tube hydrophobic strip. Sections $x = 0$ and $x = 2\pi R$ both correspond to the topmost point of the tube, while $x = \pi R$ is the bottom point, R being the tube radius. Moreover, the additional falling condition and splitting condition are implemented. According to [10], the force balance between drop weight and surface tension is written along the surface normal outward direction for the drops located near the bottom of the tube:

$$\rho\, g\, V_{drp}\cos\alpha + 2\,\pi\,\sigma\, r\,\sin^2\bar{\theta} = 0 \tag{7}$$

Bigger drops standing at the top of the tube are cut through $x = 0$ and splitted into two smaller drops if one or both of those splitted drops falls into the moving condition.

3. Hybrid surface characterization

3.1. Numerical solution of lubrication equation

The understanding of the interaction between a drop in touch with a narrow rivulet is crucial in order to access the hybrid surface behavior and ensure accurate results. In fact, larger droplets may not be

instantly absorbed by hydrophilic strips, as assumed in [10]. Thus, several simulations are run, using an Eulerian in-house solver of the well known lubrication equation. Assuming a thin liquid flowing down an inclined plate, lubrication theory gives,

$$\frac{\partial h}{\partial t} + \nabla \cdot \left(\frac{\nabla p}{3\,\mu} h^3 \right) = 0 \tag{8}$$

$$p = \rho\, g\, (h \cos\alpha - x \sin\alpha) - \Pi - \sigma\, \kappa \tag{9}$$

where x is the plate downhill direction, α is the plate inclination and h is the liquid film thickness. Disjoining pressure Π, which definition can be found in [18], is related to intermolecular forces occurring at the solid-liquid interface and requires the additional assumption of a thin precursor film. The substrate wettability (i.e. the static contact angle) can be imposed following [18, 19] and the contact angle hysteresis modeled. Capillary pressure $\sigma\,\kappa$ is related to the surface tension forces acting at the liquid-gas interface. The usual assumption of small slope approximation, $\kappa = \nabla^2 h$, is abandoned and the full expression of the free surface curvature, given in [20], is implemented,

$$\kappa = \frac{\frac{\partial^2 h}{\partial x^2}\left[1 + \left(\frac{\partial h}{\partial y}\right)^2\right] + \frac{\partial^2 h}{\partial y^2}\left[1 + \left(\frac{\partial h}{\partial x}\right)^2\right] - 2\,\frac{\partial h}{\partial x}\frac{\partial h}{\partial y}\frac{\partial^2 h}{\partial x \partial y}}{\left[1 + \left(\frac{\partial h}{\partial x}\right)^2 \left(\frac{\partial h}{\partial y}\right)^2\right]^{3/2}} \tag{10}$$

allowing to investigate static contact angles close to the mathematical limit $\theta_s < 90^\circ$ of lubrication theory. Details about space discretization can be found in [21]. An implicit $\theta-$weighted scheme is implemented for time integration due to the restrictive stability constraint, as done in [22] under the assumption of small slope approximation. The resulting sparse system is iteratively solved, at each time step. The in-house code here used was validated in [21, 23, 24] for applications involving thin liquid films flowing on flat, solid substrate.

In order to investigate the experimental test case of [9], a spherical drop standing on a vertical plate (i.e. $\alpha = 90^\circ$) is put in contact with a narrow, hydrodynamically developed rivulet. According to [9], the $L_x \times L_y$ computational domain is characterized by a given static contact angle, except for a wettable strip of width L_{FW}, where the narrow rivulet flows. The rivulet inlet section is set to $x = 0$, while fully developed condition is imposed through $x = L_x$; symmetry condition is applied through $y = 0$ and $y = L_y$.

$\rho\,(\mathrm{kg\,m^{-3}})$	$\mu\,(\mathrm{kg\,m^{-1}\,s^{-1}})$	$\sigma\,(\mathrm{N\,m^{-1}})$	$\lambda\,(\mathrm{kJ\,kg^{-1}})$
958.0	2.819×10^{-4}	5.892×10^{-2}	2256.0

Table 1. Properties of saturated liquid water at 100° C.

Liquid properties, listed in table 1, are chosen according to [9]. The initial drop base diameter is equal to $d_{b,0} = 1\,\mathrm{mm}$, which is of the same order of magnitude of the hydrophobic strip width in [9]. Since $d_{b,0}$ is less than the capillary length, $l_{cap} = \sqrt{\sigma/(\rho\, g)}$, it was reasonable to assume an initial spherical shape for the drop. Both the contact angle and the strip width are varied, in order to gain information about the influence of hybrid surface characteristics: θ_s ranges between 30° and 60°; L_{FW} up to $d_{b,0}$ is investigated. Note that the contact angle is lower than the one experimentally investigated in [9] due to lubrication limit. However, values up to 60° can be simulated thanks to the fully implementation of capillary pressure, Eq. (10). The imposed initial distance between drop center and rivulet center line is equal to $\Delta_0 = d_{b,0}/2 + L_{FW}/4$.

As clearly demonstrated by figure 1, where snapshots of the absorbed drop at successive instants are shown, it was observed that the drop is always captured by the rivulet standing on the wettable strip, independently on both the contact angle and the wettable width L_{FW}. Even if the drop gets deformed

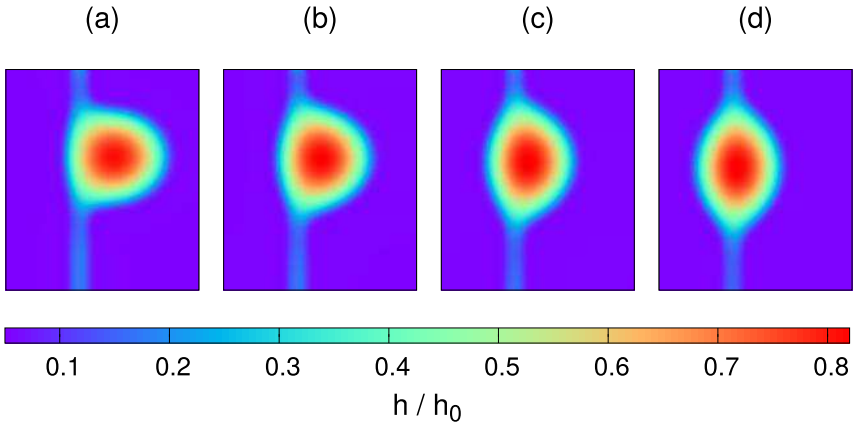

Figure 1. Absorbed drop at $t = 3.71 \times 10^{-5}$ s (a), $t = 1.04 \times 10^{-4}$ s (b), $t = 2.13 \times 10^{-4}$ s (c), $t = 4.27 \times 10^{-4}$ s (d). $L_{FW} = 0.2$ mm, $d_{b,0} = 1$ mm, $\theta_s = 60°$, $h_0 = d_{b,0} \frac{1-\cos\theta_s}{2\sin\theta_s}$.

while being absorbed, its shape keeps almost spherical when the wettable strip is thin enough. After the drop is captured, it flows along the vertical plate with a given speed, which depends on the wettable width. Thus, the whole process can be modeled as: 1) the drop is instantly captured by the rivulet flowing over the wettable strip; 2) the absorbed drop, well approximated by a spherical cap if $d_{b,0} > L_{FW}$, moves due to gravity. Assuming such a behavior, the droplet position $\mathbf{x}_{drp}$ can be traced through the definition of center of gravity:

$$\mathbf{x}_{drp} V_{drp} + \mathbf{x}_{riv} V_{riv} = \int_{L_x L_y} h \mathbf{x} \, dx \, dy \tag{11}$$

The center-rivulet position $\mathbf{x}_{riv}$ corresponds to the known center of the wettable strip; V_{drp} is equal to the initial drop volume (spherical cap with base diameter $d_{b,0}$ and contact angle θ_s); V_{riv} is the initial volume of the fully developed rivulet; the integral term at the RHS is computed from the numerical liquid distribution. Thus, the drop advection velocity $u_{drp} = \frac{dx_{drp}}{dt}$ can be easily estimated as well as the absorption time, defined as t_{abs} : $|y_{drp} - y_{riv}| \leq 0.01\,\Delta_0$.

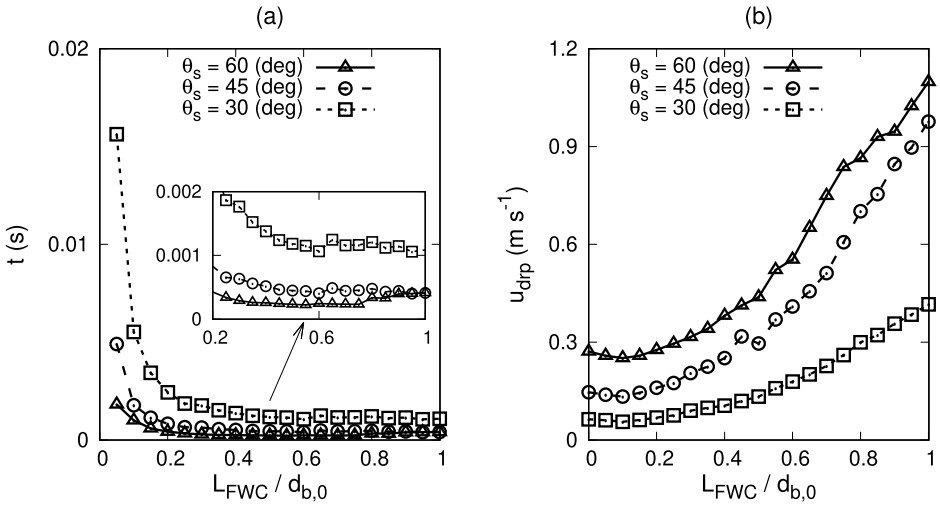

Figure 2. Computed drop absorption time (a) and absorbed drop velocity (b) as a function of wettable width L_{FW} and static contact angle. $d_{b,0} = 1$ mm.

Figure 2(a) traces the absorption time required by the drop to be captured by the wettable strip. As expected, a larger wettable width leads to a decrease in t_{abs}. It is also important to point out that the absorption process is almost instantaneous for low substrate wettability: $t_{abs} < 5 \times 10^{-3}$ s when $\theta_s = 60°$. The absorbed drop advection velocity is plotted in figure 2(b). It can be stated that u_{drp} approaches the filmwise velocity for increasing wettable width. Drops spreading on lower wettable substrate move faster due to the higher volume (meaning an higher driving gravity force) of the initial drop.
Such information are used to parameterize the hydrodynamic behavior of hybrid substrate and add the strip effect in the Lagrangian solver, as explained in the next section.

3.2. Modeling of hydrophilic strips

The Eulerian simulations of hybrid patterned surfaces suggest that the drop is always captured by the hydrophilic strips: if $L_{FWC} \geq d_b$, the drop is fully incorporated by the filmwise liquid pattern flowing over the hydrophilic region; if $L_{FWC} < d_b$, the drop hold an almost spherical shape. A continuous film pattern is assumed over the whole hydrophilic region. It was also shown that the absorption process can be considered (from a numerical point of view) an instantaneous event when the hydrophobic region is characterized by an high value of the contact angle. The Lagrangian solver first looks for drops touching the hydrophilic strips. Thus, two cases may occur:

a) if $d_b \leq L_{FWC}$, the absorbed drop is simply deleted from the computational domain;
b) if $d_b > L_{FWC}$, the solver retains the drop and its center of gravity is moved along the center-line of the closer hydrophilic strip, located at $y = -L_{FWC}/2$ or $y = L_{DWC} + L_{FWC}/2$.

As previously pointed out, the external forces acting on a drop induce an hysteresis in the contact angle along wetted perimeter and eventually lead to drop motion. However, when case b) occurs, a portion of drop stands on an already wetted pattern and the calculation of rigidity force due to surface tension must be modified. Assuming that the rigidity force F_σ only acts along the dry perimeter of the drop, it can be rewritten as,

$$F_\sigma = d_b \int_\phi^{\pi-\phi} \sigma \cos\theta \cos\psi \, d\psi, \; \sin\phi = \frac{L_{FWC}}{d_b} \tag{12}$$

ϕ corresponding to the dry arc of drop perimeter and $\theta(\psi)$ being modeled according to [13, 14].
Calculating the rigidity force through Eq. (12) and solving the power balance following [1, 17], it can be verified that the resulting drop velocity u_{drp} increases with the L_{FWC}/d_b ratio, according to the numerical results of figure 2(b). Thus, both the drop moving condition and the drop advection velocity calculation are modified according to Eq. (12) for all the absorbed drops having $d_b > L_{FWC}$.

4. Validation and results

The following results are focused on condensation heat transfer optimization around a condenser tube of radius R, characterized by an hybrid surface, L_{DWC} and L_{FWC} denoting the hydrophobic width and the hydrophilic width. The experimental setup of [9] is replicated. Thus, liquid properties listed in table 1 are considered and a tube of radius $R = 3.175$ mm is simulated, the hydrophobic width ranging between 0.6 mm to 1 mm. Advancing and receding contact angles are set to $\theta_a = 135°$ and $\theta_r = 56°$.
Figure 3 shows the drop distribution over the unwrapped domain (including both the hydrophobic and the hydrophilic regions) at 5 successive time steps. We can see a big droplet at the topmost point of the tube splitted between $x = 0$ and $x = 2\pi R$, according to the implemented periodic condition. Also, some droplets touching the hydrophilic strips are absorbed; the bigger ones are moved along the hydrophilic strip center-line. Such droplets will drain due to gravity force, drying part of the computational domain and ensuring free nucleation spots. Since the whole hydrophobic strip can be simulated, a quantitative validation with experimental results of [9] is tried. Thus, we simulate different configurations. The hydrophobic width is fixed to $L_{DWC} = 0.6$ mm, while L_{FWC} is varied, looking for the best configuration in terms of computed heat flux. Different substrate subcoolings are investigated, namely $\Delta T_{sc} = 5°$C, 6°C

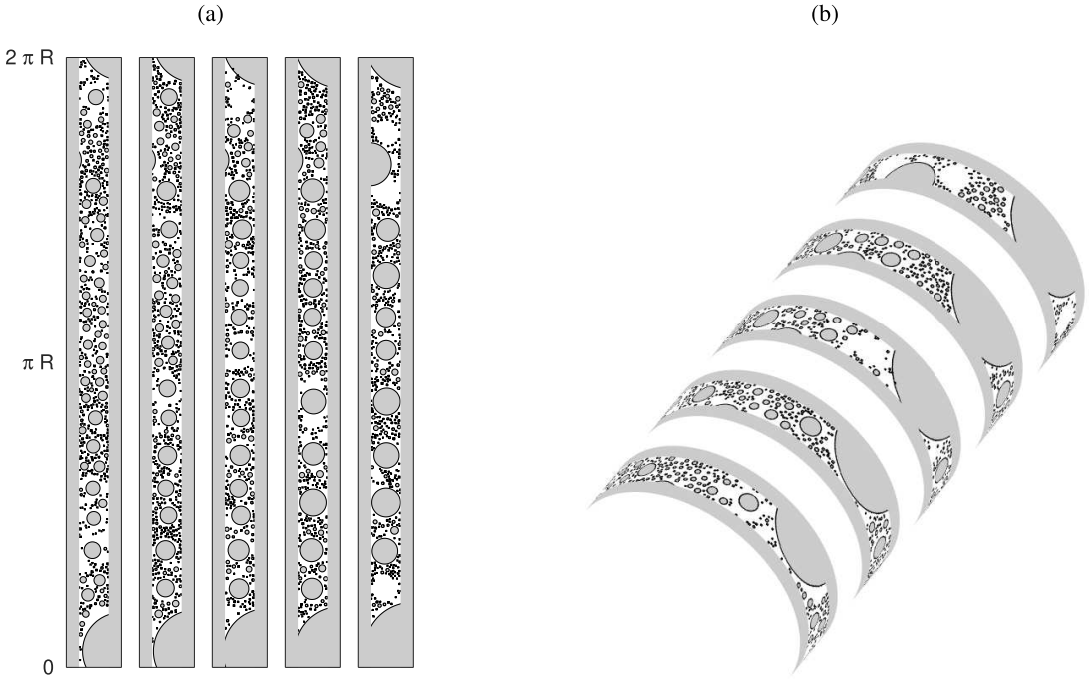

Figure 3. Drop distribution over the hybrid surface at five successive time steps (0.91 seconds apart): unwrapped surface, $x = 0$, $2\pi R$ being the topmost point and $x = \pi R$ the bottom-most point (a); 3D view (b). $L_{DWC} = 1\,\text{mm}$, $L_{FWC} = 0.8\,\text{mm}$, $\theta_a = 135°$, $\theta_r = 56°$, $\Delta T_{sc} = 10°\text{C}$, $N = 10^8\,\text{m}^{-2}$.

and 9°C, corresponding to the imposed values of condensing mass flow rate per unit free-surface area, $\dot{m}''_c = q''_c/\lambda$. Final time is set to $t_f = 30\,\text{s}$, ensuring that a sufficient number of wetting-dewetting cycles are simulated. Assuming that condensation drives heat transfer process, the heat flux is computed as,

$$q'' = \frac{\dot{m}''_c\,\lambda}{L_{FWC} + L_{DWC}} \left(L_{FWC} + \frac{1}{t_f} \int_0^{t_f} \sum_i \frac{S_{drp,i}}{2\,\pi\,R}\,dt \right) \tag{13}$$

$S_{drp,i}$ being the free surface area of the i-th population drop. The nucleation density depends on both the micro-structure of the solid surface and the imposed subcooling. Since Eq. (1) offers only an upper limit for the actual nucleation density, N as a function of ΔT_{sc} is determined in order to best fit the experimental results: fixing the imposed ΔT_{sc}, parametric simulations are run varying N and the heat flux is computed for different configurations ($L_{FWC} = 0.2, 0.3, 0.4, 0.5, 0.6\,\text{mm}$) and compared with the experimental values of [9]; the chosen nucleation density for a given subcooling corresponds to the minimum sum of square of errors in the computed q'' for the investigated configurations L_{FWC}. Figures 4(a) and 4(b), referred to $\Delta T_{sc} = 5°\text{C}$ and 6°C, reveal a good agreement between experimental and numerical results, while a bit more uncertainty is obtained for $\Delta T = 9°\text{C}$, figure 4(c). However, the correct optimum configuration at $L_{FWC} = 0.3\,\text{mm}$ is always replicated, meaning that the mathematical model is able to catch the main physics behind condensation on hybrid surfaces. Also, reasonable values of the nucleation density were obtained. A 10% variation in N does not change the maximum position, while producing a heat flux variation comparable to the experimental uncertainty of 9% declared in [9].

5. Conclusion

A Lagrangian model describing the evolution of droplets condensing on a hybrid (both plane or cylindrical) surface was presented. Basic mechanisms such as nucleation, growth, coalescence, shedding,

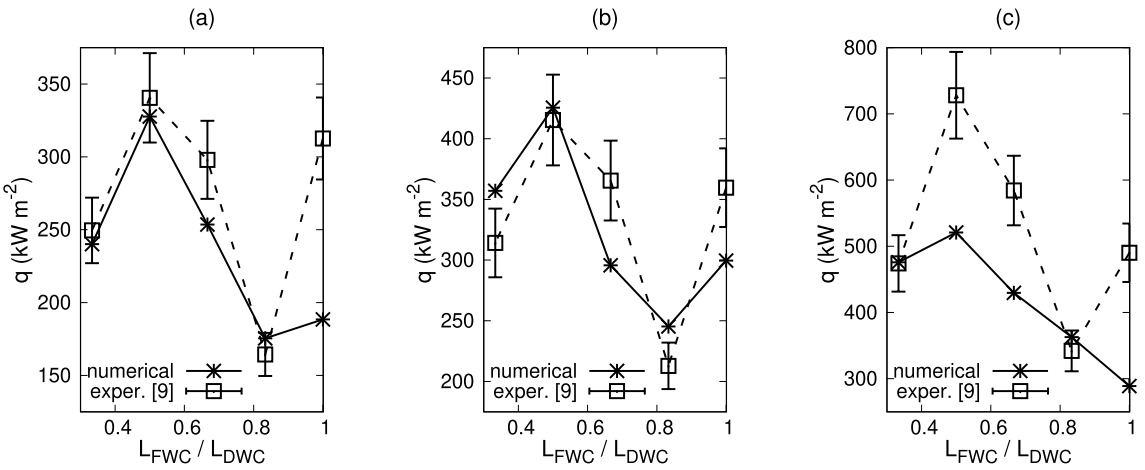

Figure 4. Computed vs experimental [9] heat flux as a function of hydrophilic width: $\Delta T_{sc} = 5°\mathrm{C}$, $N = 1.1 \times 10^9\,\mathrm{m}^{-2}$ (a); $\Delta T = 6°\mathrm{C}$, $N = 1.0 \times 10^9\,\mathrm{m}^{-2}$ (b); $\Delta T = 9°\mathrm{C}$, $N = 1.25 \times 10^9\,\mathrm{m}^{-2}$. $L_{DWC} = 0.6\,\mathrm{mm}$.

fall are implemented, allowing for a realistic description of the liquid pattern details. Running fully Eulerian simulations, it was possible to understand the drop migration process and add the effect of hydrophilic strips in the Lagrangian model. Averaged engineering relevant quantities, such as heat flux, may, thus, be predicted. The model was validated simulating practical problems involving heat transfer over hybrid surfaces, showing that the main physical features are correctly captured. In particular, the existence of an optimal geometry configuration was observed and its location correctly predicted, according to literature experimental data [8, 9], thanks to the model improvements. However, numerical results are affected by some physical parameters given as input of the Lagrangian solver: nucleation density, which was set in order to fit experimental data due to its difficult estimation, greatly influences the liquid pattern evolution.

References

[1] De Candido E, Croce G and D'Agaro P 2012 *Heat Transfer Eng.* **33** 1130–1137
[2] Croce G, De Candido E, Habashi W G, Munzar J, Aube M, Baruzzi G S and Aliaga C 2010 *J. Aircraft* **47** 1283–1290
[3] Durán I R and Laroche G 2019 *Prog. Mater. Sci.* **99** 106–186
[4] Durán I R and Laroche G 2019 *Adv. Colloid Interface Sci.* **263** 68–94
[5] Croce G, D'Agaro P, De Angelis A and Mattiello F 2007 *IMechE, Part D: J. Automobile Eng.* **221** 1241–1250
[6] D'Agaro P, Croce G and Cortella G 2006 *Appl. Therm. Eng.* **26** 1927–1934
[7] Bisetto A, Torresin D, Tiwari M K, Del Col D and Poulikakos D 2014 *J. Phys. Conf. Ser.* **501** 012028
[8] Peng B, Ma X, Lan Z, Xu W and Wen R 2015 *Int. J. Heat Mass Transfer* **83** 27–38
[9] Alwazzan M, Egab K, Peng B, Khan J and Li C 2017 *Int. J. Heat Mass Transfer* **112** 991–1004
[10] Croce G, D'Agaro P and Suzzi N 2019 *Proc. 17th ICNMM* (ASME) https://doi.org/10.1115/ICNMM2019-4291
[11] Rose J W 1976 *Int. J. Heat Mass Transfer* **19** 1363–1370
[12] Liu X and Cheng P 2015 *Int. J. Heat Mass Transfer* **83** 842–849
[13] El Sherbini A I and Jacobi A M 2004 *J. Colloid Interface Sci.* **273** 556–565
[14] El Sherbini A I and Jacobi A M 2004 *J. Colloid Interface Sci.* **273** 566–575
[15] El Sherbini A I and Jacobi A M 2006 *J. Colloid Interface Sci.* **299** 841–849
[16] El Sherbini A I and Jacobi A M 2006 *ASME J. Heat Transfer* **128** 427–433
[17] Kim H, Lee H J and Kang B H 2002 *J. Colloid Interface Sci.* **247** 372–380
[18] Schwartz L W and Eley R R 1998 *J. Colloid Interface Sci.* **202** 173–188
[19] Zhao Y and Marshall J S 2006 *J. Fluid Mech.* **559** 355–378
[20] Do Carmo M P 1976 *Differential Geometry of Curves and Surfaces* (Englewood Cliffs, New Jersey: Prentice-Hall, Inc.)
[21] Suzzi N and Croce G 2017 *J. Phys. Conf. Ser.* **796** 012038
[22] Diez J A and Kondic L 2002 *J. Comput. Phys.* **183** 274–306
[23] Suzzi N and Croce G 2017 *J. Phys. Conf. Ser.* **923** 012020
[24] Suzzi N 2018 *Numerical simulation of thin liquid films over a solid non-wettable substrate assuming lubrication approximation* Ph.D. thesis Università degli Studi di Udine